

Modified DEBA for determining size dependent shear fracture energy of laminates

M. Saeed Goodarzi¹ and Hossein Hosseini-Toudeshky^{*2}

¹ Department of Industrial, Mechanical and Aerospace Engineering, Buein Zahra Technical University, Buein Zahra, Qazvin, Iran

² Department of Aerospace Engineering, Amirkabir University of Technology, No. 424, Hafez Ave. Tehran, Iran

(Received April 21, 2017, Revised April 18, 2018, Accepted May 25, 2018)

Abstract. It has been argued that fracture energy of composite laminates depends on their thickness and number of layers. In this paper a modified direct energy balance approach (DEBA) has been developed to evaluate the mode-II shear fracture energy for E-glass/Epoxy laminates from finite element model at an arbitrary thickness. This approach considers friction and damage/plasticity deformations using cohesive zone modeling (CZM) and nonlinear finite element modeling. The presence of compressive stress and resulting friction was argued to be a possible cause for the thickness dependency of fracture energy. In the finite element modeling, CZM formulation has been developed with bilinear cohesive constitutive law combined with friction consideration. Also ply element have been developed with shear plastic damage model. Modified direct energy balance approach has been proposed for estimation of mode-II shear fracture energy. Experiments were performed on laminates of glass epoxy specimens for characterization of material parameters and determination of mode-II fracture energies for different thicknesses. Effect of laminate thickness on fracture energy of transverse crack tension (TCT) and end notched flexure (ENF) specimens has been numerically studied and comparison with experimental results has been made. It is shown that the developed numerical approach is capable of estimating increase in fracture energy due to size effect.

Keywords: composite; fracture energy; finite element method; Mode-II shear; damage

1. Introduction

Analysis of delamination growth has been studied by several researchers through different methods. Methods based on the fracture mechanics approach has been used to predict growth of an existed crack. Methods such as virtual crack closure technique (VCCT) (Rybicki and Kanninen 1977, Krueger 2004) have been widely used to calculate the energy release rate at delamination front. Analytical models have also used in the simulation of interfacial debonding (Achillopoulou *et al.* 2016, Bocciarelli *et al.* 2016 and Girot *et al.* 2017). Moreover, methods based on the continuum damage mechanic approach such as cohesive zone modeling have been advanced to predict both initiation and growth of cracks. Cohesive elements use traction-separation laws incorporating energy and strength based criteria at any point of interface without prior information about location of crack and growth path. The original cohesive fracture concept was proposed by Barenblatt (1959, 1962) who considered additional cohesive forces to hold the upper and lower surfaces of a narrow interface ahead of the crack tip and removed the singularity. Most of the advances in the implementation of this model into numerical methods have taken place during the last decade. Camanho *et al.* (2003) presented an interface element of cohesive zone method.

The element contained bilinear constitutive law in order to simulate growth of delamination in mixed-mode bending specimen. Turon *et al.* (2007) expanded this method to simulate growth of delamination under tensile fatigue loadings. Hosseini-Toudeshky *et al.* (2013) proposed finite element models to simulate the growth of delamination of post-buckled laminates under fatigue loading. Shiming and Huifen (2012) investigated the effect of debonding separation at the steel-concrete interface using three-dimensional nonlinear finite element model of concrete-filled steel tube composite. It was shown that the load carrying capacity dropped with the increasing the size of the gap. Kharazan *et al.* (2014) used cohesive elements for the simulation of delamination growth in composite laminates under low velocity impact. The efficiency of the presented approach was shown in term of accuracy of results and simulation time. Hosseini-Toudeshky *et al.* (2015) also simulated damage propagation within composite and metal joint in wind turbine blade under fatigue loading. Kim *et al.* (2015) used cohesive elements to investigate debonding concrete and fiber reinforced polymer with layers in tapered form. Reasonable agreement was shown between experimental and predicted results.

Cohesive elements are being used in simulation of friction at cracked zone. Tvergaard (1990) presented an interface model for fiber-matrix debonding that neglects the friction as long as the interface damage is not completed and considers friction law when complete de-cohesion is attained. Shi and Soutis (2016) simulated four point bend specimen using contact pairs with friction between internal

*Corresponding author, Professor,
E-mail: hosseini@aut.ac.ir

^a Adjunct Professor, E-mail: mgoodarzi@aut.ac.ir

plies that is independent from interlaminar damage evolution. Chaboche *et al.* (1997) modified Tvergaard interface law by introducing a friction term before complete de-cohesion in order to eliminate physical inconsistencies of that model. Lin *et al.* (2001) considered two uncoupled bilinear laws for the normal and tangential stresses and considered the tangential stress smaller than the modulus of the normal stress times to the friction coefficient. Alfano and Sacco (2006) proposed a novel method to combine cohesive friction and damage in interface elements. They assumed that friction occurs only on the fully damaged part. Fiber push-out test and a masonry wall loaded in compression and shear were simulated and compared the results with the available experimental results.

Fracture energy is an important parameter that has been studied by many researchers. Wisnom (1992) and Cui *et al.* (1994) evaluated size dependent fracture energy for transverse crack tension test (TCT) under quasi-static applied loads. They suggested the main possible reasons for the size effect. In the first paper (Wisnom 1992), crack tip plastic deformations were mentioned as the reason for thickness dependency of fracture energy. In the other one (Cui *et al.* 1994), compressive stresses that appear on the crack surface were mentioned as another possible reason for the size effect. Van der Meer and Sluys (2013) presented a numerical study on the hypotheses from Wisnom (1992) and Cui *et al.* (1994) from which cohesive zone modeling was used containing shear nonlinearity for layers and friction on surfaces of the crack. Van der Meer and Sluys (2013) simulated the experiments reported by Cui *et al.* (1994) and reasonable agreement with the measured size effect was shown. However, in this numerical investigation by Van der Meer and Sluys (2013), fracture energy of finite element model has been calculated by a relationship under the assumption of linear elastic fracture mechanics whilst the of plastic deformations in the model are considerable.

Sun and Davidson (2006) evaluated the geometric nonlinearities and friction effects on fracture energy ENF tests. They analyzed the sensitivity of fracture energy to the span length, coefficient of friction along the crack plane and roller diameter. Davidson *et al.* (2007) also performed ENF experiment and examined the effect of fixture compliance on perceived toughness. They developed a direct energy balance approach (DEBA) (Sun and Davidson 2005) to calculate the fracture energy by two-dimensional nonlinear finite element analysis considering the effects of friction and large deformations. The work of friction in the Sun and Davidson's formulation is calculated by the use of average tangential forces on nodes during crack advancement.

In the present study, a modified DEBA has been introduced that uses a nonlinear finite element model containing friction in interface elements and shear nonlinearity for ply elements to consider the effects of specimen thickness on the perceived toughness of composite laminates in mode-II. In the interface element, damage evolution proceeds according to the bilinear cohesive constitutive law in combination with friction up to the complete de-cohesion. In the ply elements shear damage-nonlinearity is applied to the shear strain component. The contributions of the present modified

DEBA over the previous approach is that the work of friction in this approach has been directly removed from the strain energy at cohesive constitutive law. Whilst in the previous approach, using the average of tangential forces before and after crack advance increase the numerical errors. Moreover the dissipation of energy due to shear nonlinearity of the lamina at the vicinity of the interface has been included in the strain energy at the ply elements. These advantages make the capability of estimating numerically the shear fracture energies of laminates with higher thickness using experimental fracture energy of a low thickness laminate. Fracture energy are calculated for E-glass/Epoxy unidirectional composite laminate using modified DEBA for TCT and ENF specimens and the results are compared with the performed experiments on ENF specimens and available results from previous experiments on TCT specimens.

2. Finite element formulation

In the nonlinear finite element model of the present study, the plies are modeled as a continuum with a nonlinear plasticity law for shear deformation, while the interface is modeled with cohesive damage containing friction.

2.1 Interface element formulation

In the present study interface element has been considered with cohesive constitutive law containing friction. After the strain reaches the critical value of damage initiation, damage evolution proceeds according to the cohesive constitutive law in combination with coulomb friction up to the complete de-cohesion of the cohesive zone according to the assumption made by Alfano and Sacco (2006). Though, in the present model the formulation is in the form of stress-strain relation because of small thickness interface element used in the simulations. In this model it has been assumed that the damaged area (A) in the damaged cohesive zone that corresponding to an integration point is broken down into two domains, the un-cracked area (A_u) with the cohesive damage and cracked area (A_c) with friction, where

$$A = A_c + A_u \quad (1)$$

From which

$$A_c = dA \quad \text{and} \quad A_u = (1 - d)A \quad (2)$$

Where d is the damage variable of interface element which has been defined as the ratio of cracked area to the total area. It has been assumed that the strain is similar for both area. Hence, $\underline{\epsilon}^u$ and $\underline{\epsilon}^c$ are the strain vectors on the two domains A_u and A_c , respectively. It follows as

$$\underline{\epsilon} = \begin{bmatrix} \epsilon \\ \gamma \end{bmatrix} = \underline{\epsilon}^u = \underline{\epsilon}^c \quad (3)$$

In this equation, ϵ and γ are two components of strain

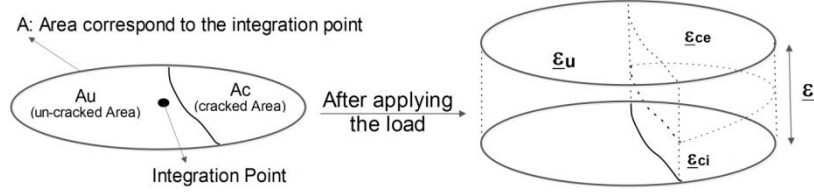


Fig. 1 Schematic representation of strain on the area of an integration point

$\underline{\epsilon}^c$). Fig. 1 schematically presents the strain on the area of an integration point. For the cracked strain, $\underline{\epsilon}^c$, the strain contains from two parts of elastic ($\underline{\epsilon}^{ce}$) and inelastic ($\underline{\epsilon}^{ci}$)

$$\underline{\epsilon}^c = \underline{\epsilon}^{ce} + \underline{\epsilon}^{ci} = \begin{bmatrix} \epsilon^{ce} + \epsilon^{ci} \\ \gamma^{ce} + \gamma^{ci} \end{bmatrix} \quad (4)$$

On the other hand, the strain on the un-cracked area is totally elastic

$$\underline{\epsilon}^u = \underline{\epsilon}^{ue} = \underline{\epsilon} \quad (5)$$

It has been assumed that on either domains of the damaged interface, strain is constant, while stress is generally different on the cracked and un-cracked domains. On the un-cracked domain the stress follows as

$$\underline{\sigma}^u = \begin{bmatrix} \sigma^u \\ \tau^u \end{bmatrix} = \mathbf{K} \underline{\epsilon} \quad (6)$$

In this equation σ^u and τ^u components of the un-cracked area stress ($\underline{\sigma}^u$) and \mathbf{K} is stiffness diagonal matrix of normal and shear

$$\mathbf{K} = \begin{bmatrix} K_1 & 0 \\ 0 & K_2 \end{bmatrix} \quad (7)$$

On the cracked of cohesive interface, stress is calculated using $\underline{\epsilon}^{ci}$ by the following relationship

$$\underline{\sigma}^c = \begin{bmatrix} \sigma^c \\ \tau^c \end{bmatrix} = \begin{bmatrix} (1 - h(\epsilon - \epsilon^{ci})) K_1 & 0 \\ 0 & K_2 \end{bmatrix} (\underline{\epsilon} - \underline{\epsilon}^{ci}) \quad (8)$$

Where K_1 and K_2 , normal and shear interface stiffness equal to the normal stiffness and initial shear stiffness of lamina, E_2 and G_{12} respectively. In this equation σ^c and τ^c are two components of stress in the cracked area $\underline{\sigma}^c$ and the Heaviside function $h(x)$ defines as

$$h(x) = \begin{cases} 1 & \text{if } x \geq 0 \\ 0 & \text{if } x < 0 \end{cases} \quad (9)$$

Where x defined as $(\epsilon - \epsilon^{ci})$ in Eq. (8). Then the total stress will be homogenized by weighting the stress in the cracked area and un-cracked area using the damage variable

$$\underline{\sigma} = \begin{bmatrix} \sigma \\ \tau \end{bmatrix} = d \underline{\sigma}^c + (1 - d) \underline{\sigma}^u \quad (10)$$

Where σ and τ are two components of the total stress. To define the inelastic strain of cracked area, friction function defines as

$$\phi(\underline{\sigma}^c) = \mu \sigma^c + |\tau^c| \quad (11)$$

Where, μ is the friction coefficient. It worth mentioning that σ^c is always non-positive according to Eq. (8). The evolution of inelastic strain of cracked area governs by the following non-associative equation

$$\underline{\dot{\epsilon}}^{ci} = \begin{bmatrix} \dot{\epsilon}^{ci} \\ \dot{\gamma}^{ci} \end{bmatrix} = \dot{\lambda} \begin{bmatrix} 0 \\ \frac{\partial \phi}{\partial \tau^c} \end{bmatrix} = \dot{\lambda} \begin{bmatrix} 0 \\ |\tau^c| \end{bmatrix} \quad (12)$$

Where multiplier $\dot{\lambda}$ is uniquely defined with the additional Kuhn-Tucker conditions

$$\dot{\lambda} \geq 0, \quad \phi(\underline{\sigma}^c) \leq 0, \quad \dot{\lambda} \phi(\underline{\sigma}^c) = 0 \quad (13)$$

Since at the beginning $\underline{\epsilon}^{ci} = 0$, it can be concluded that the normal component of $\underline{\epsilon}^{ci}$ vector, ϵ^{ci} , is always equal to zero.

The evolution of damage parameter in Eqs. (2) and (10) drives the following bilinear equation

$$d = \frac{\gamma^f (\alpha - \gamma^0)}{\alpha (\gamma^f - \gamma^0)} \quad (14)$$

Where α is the maximum applied γ in all previous iterations. γ^f is the complete de-cohesion strain in shear and defines by

$$\gamma^f = (2G_{IIc}) / (h_0 \tau_0) \quad (15)$$

Where G_{IIc} is the fracture energy in mode-II. τ_0 is shear strength of laminate. h_0 is thickness of the interface element and initiation strain (γ^0) defines as follows

$$\gamma^0 = \frac{\tau^0}{G(0)} \quad (16)$$

2.2 Ply model with plasticity

The damage/plasticity model for shear nonlinearity proposed by Van Paepegem *et al.* (2006) for in-plane shear behavior is used here. Under the assumption of transverse isotropy of lamina, this model is used as the out of plane shear stress. The model relates the shear stress, τ , to the shear strain, γ , as

$$\tau = (1 - d_L)(\gamma - \gamma^p)G \quad (17)$$

Where d_L is the damage variable of lamina and G is the initial shear stiffness and γ^p is the plastic shear strain.

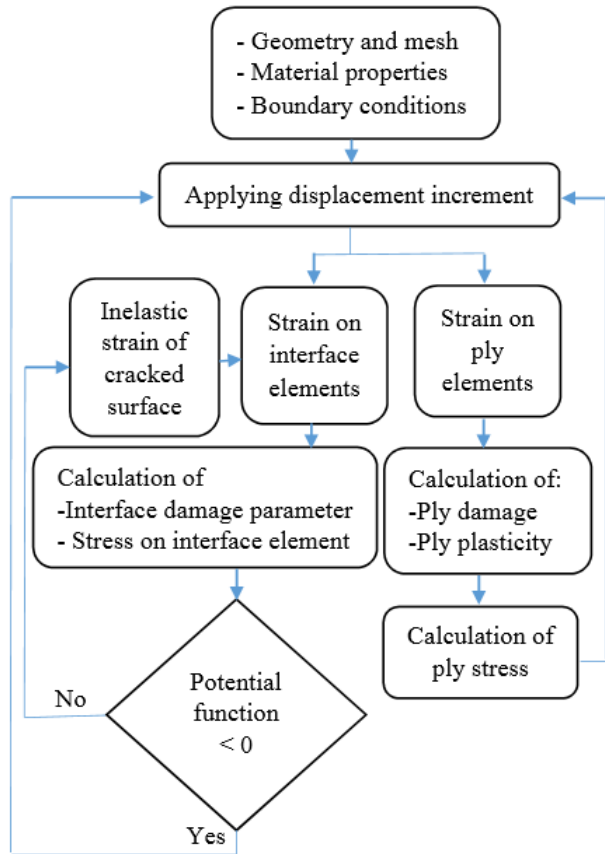


Fig. 2 Flowchart of interface and ply elements

Damage and plastic strain evolve as a function of the strain

$$\gamma^p = \frac{\ln\left(1 + \frac{c_1 c_2 \bar{\gamma}^2}{2}\right)}{c_2} \quad (18)$$

$$d_L = \frac{\ln(1 + c_3 c_4 \bar{\gamma})}{c_4} \quad (19)$$

Where, c_1 to c_4 are material parameters that can be used to fit an experimental stress-strain curve including unloading/reloading behavior. The history variable $\bar{\gamma}$ is defined as the maximum history value of γ with the following equation.

$$\bar{\gamma}(t) = \max_{t'=0}^{t'=t} \gamma(t') \quad (20)$$

Using the maximum of history values of shear strain ensures that when unloading occurs in the wake of the crack, stress decreases with respect of the reduced stiffness, $(1 - d_L)G_{xz}$, and that the plastic strain γ^p is permanent.

The flowchart of formulation within finite element model of interface and ply elements have been illustrated in Fig. 2.

2.3 Evaluation of fracture energy from finite element

The Direct Energy Balance Approach proposed by Sun and Davidson (2005). This method uses the Griffith relation

for the energy release rate along with an additional term to account the work of frictional dissipation during crack advancement. The work of frictional dissipation in the Sun and Davidson's formulation is calculated by sum of products of the average tangential forces (before versus after crack advancement) and the corresponding sliding displacements of nodes during crack advancement. Using the average of tangential forces may increase the numerical errors. In the presented modified direct energy balance approach, the work of friction dissipation has been deducted directly from the strain energy. Moreover in the present model the energy dissipation due to shear plastic deformation in the ply near the interface has been included in the strain energy obtained from FE model. The fracture energy is determined by the following equation

$$G_{IIC} = \frac{1}{B} \left[\frac{\partial(W_e - U)}{\partial a} \right] \quad (21)$$

Where, W_e is the work of external forces, U is the strain energy, B is the width of specimen and ' a ' is crack length. Since at the point of load drop, crack propagation occurs at approximately constant load, W_e is negligible and the Eq. (21) reduces to

$$G_{IIC} = -\frac{(U_{a+\delta a} - U_a)}{B\delta a} \quad (22)$$

In the above equation, U_a is the obtained strain energy by FE analysis of the body containing the initial crack length (a), and $U_{a+\delta a}$ is the strain energy after the crack advance (at crack length of $a+\delta a$). From which δa is crack advance.

3. Experimental results

3.1 End notched flexure tests

In this section, obtained results of experimental tests on ENF specimens based on ASTM D7905/D7905M-14 (2014) with different thicknesses are presented. The laminates are made of E-glass/epoxy by Vacuum Infusion Process (VIP). All layers were in zero ply angles. Initial crack is performed using a non-adhesive insert. For the ENF tests, specimens were cut out from prepared laminate with a water jet. The length and width of the ENF specimens were 160 mm and 20 mm respectively. The specimens are in

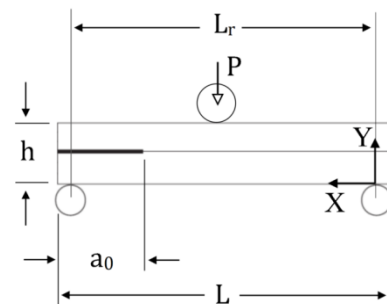


Fig. 3 Geometry of ENF specimen



Fig. 4 The ENF test apparatus and fixture used in the experiments

Table 1 Obtained fracture energy of E-glass/epoxy ENF specimens from experiments

Laminate	Thickness (mm)	G_{IIc} (N/mm)
10 Ply	2.5	0.802
16 Ply	4	0.973
22 Ply	5.5	1.092

three thicknesses of 5.5 mm (22 layers), 4 mm (16 layers) and 2.5 mm (10 layers). The ENF specimen has been present schematically in Fig. 3. In this figure, a_0 denotes

the initial crack length of specimen and L_r is supporting rollers distance and L is total specimen length. In the ENF tests a_0 was 30 mm and L_r was 100 mm. The supporting rollers and loading roller diameters were 10 mm. ENF tests are performed under applied displacement rate of 0.008 mm/s. The test procedure is outlined in ASTM D7905/D7905M-14 (2014).

The ENF test apparatus and fixture are shown in Fig. 4. The results of obtained fracture energy for non pre-cracked ENF specimens are listed in Table 1. It can be observed from the experiments that by increasing the thickness of laminate from 10 layers to 22 layers, the obtained initiation value of fracture energy increases for 36%.

3.2 Characterization tests

Tension tests have been performed for the characterization of E-glass/epoxy material. The length, width and thickness of the tension specimens were 200 mm, 20 mm and 4 mm respectively. Laminates with 16 ply of zero angle orientation used for determination of longitudinal and transverse modulus and poisson's ratio. Moreover, Laminates with 16 ply of 45° angle orientation used for determination of shear modulus, shear strength and c_1 to c_4 curve-fitting parameters of damage/plasticity model that have been used in Eqs. (18) and (19). c_1 to c_4 material parameters are in Eqs. (17) to (19). c_1 to c_4 parameters have been obtained using curve-fitting tool in MATLAB software. The R-square value of curve fitting is 0.993. The obtained material properties and parameters are listed in

Table 2 Material properties and parameters for E-glass/epoxy obtained by experiments

E_1 (GPa)	E_2 (GPa)	ν_{12}	G_{12} (GPa)	S (MPa)	C_1	C_2	C_3	C_4
19.29	19.29	0.20	2.27	60	31.4	22.82	3.954	0.4502

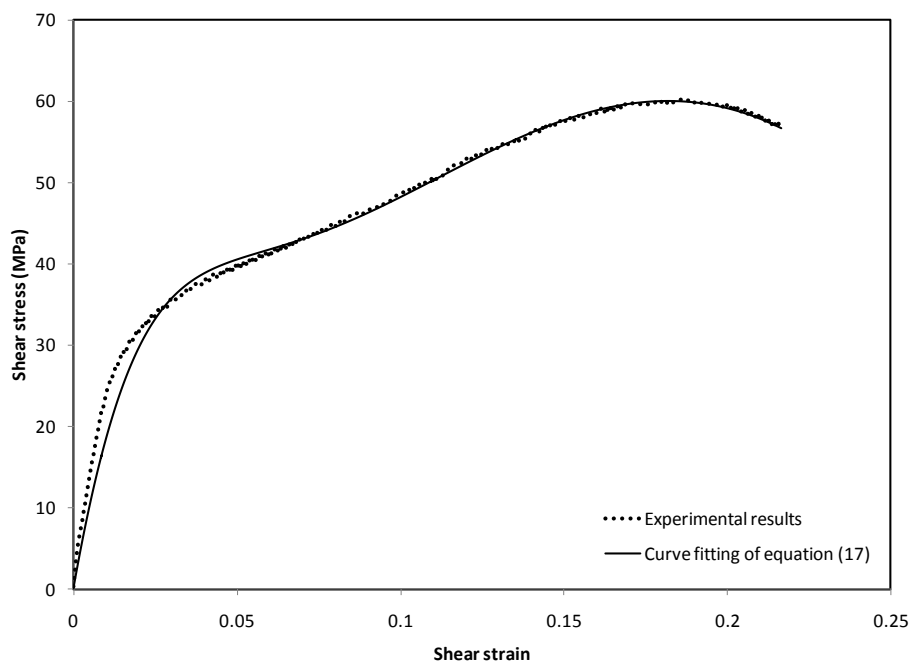


Fig. 5 Experimentally determined shear stress vs. strain for E-glass/epoxy material

Table 2. The diagram of experimental shear stress versus strain and curve fitting are shown in Fig. 5.

4. Numerical results

The described formulation for ply and interface elements has been implemented in ANSYS finite element software as user programmable features. In this section finite element analyses for one element model, ENF specimens and transverse crack tension test are performed to verify the presented model and also to study the size effect.

4.1 One element model

In this section, a model containing two lamina elements with one interface element between them is presented. The Geometry and boundary conditions of the model are illustrated in Fig. 6. The mechanical properties of lamina and the interface element material properties are experimental parameters for E-glass/913 epoxy which have

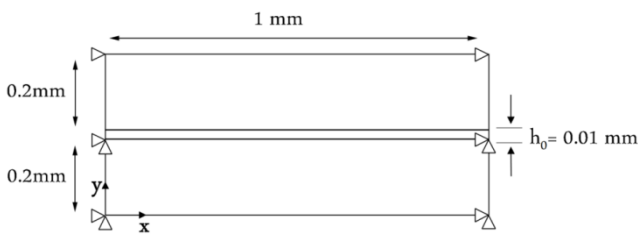


Fig. 6 Geometry and boundary conditions of one element model

been listed in Table 3.

The lower element has been fully constrained in x and y direction and the upper element can gradually move in the x direction causing the xy shear strain on interface element to increase from zero to 2. Normal pressure of 10 MPa at $y = 0.41$ mm in y direction has been applied to the upper element to activate the friction in one element model. Note that in the ENF simulations, the normal pressure that activates the friction is naturally induced by stress field. Three different friction coefficients of 0, 0.3 and 0.6 have been also considered to study the effect of friction coefficient (μ) on constitutive behavior of interface element. The obtained results for three different friction coefficients are presented in Fig. 7. The differences between the obtained stress-strain response for zero friction coefficient and two other curves after damage initiation, show the dependency of friction shear stress to the inelastic strain of cracked area due to friction as described by Eq. (12).

4.2 End notched flexure simulation

In this section, the ENF test has been simulated with described formulations and method. The Dimensions of the specimen and fixture are the same as experiments. All rollers were modeled as rigid surfaces. The mechanical properties and parameters used for simulations are listed in Table 2. Contact elements have been used between rollers and specimen. The experimentally obtained kinetic friction coefficients of laminate cracked interfaces, faces of initial delamination and laminate-roller contacts are 0.6, 0.48 and 0.4 respectively.

The friction coefficients are obtained by angle of response method which is schematically shown in Fig. 8. In

Table 3 Material properties, friction coefficient and input fracture toughness for E-glass/913 epoxy from Cui *et al.* (1994) and Van der meer and Sluys (2013)

E_1 (GPa)	E_2 (GPa)	ν_{12}	G_{12} (GPa)	S (MPa)	G_{IIC} (N/mm)	μ	C_1	C_2	C_3	C_4
43.9	15.4	0.30	5.8	75	0.7	0.65	25	-34	46	-4

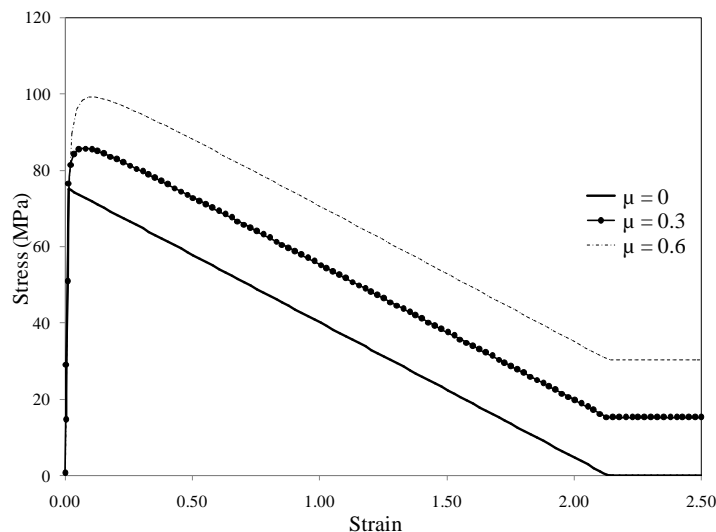


Fig. 7 Effect of friction coefficient on the stress-strain response of one element model

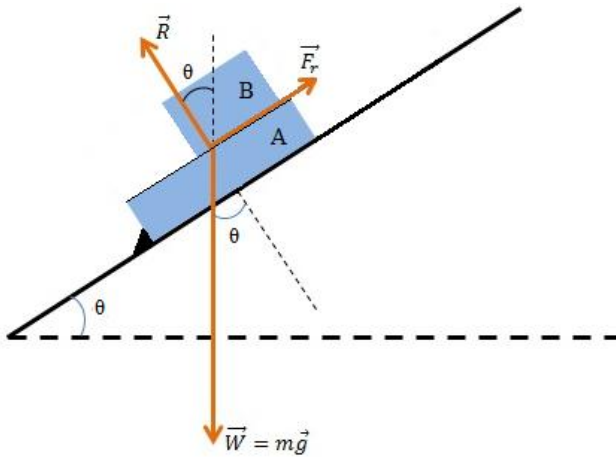


Fig. 8 Angle of response method for determination of friction coefficients

this figure, \vec{W} is weight of B , \vec{R} is normal reaction of A and B contacts and \vec{F}_r is friction of A and B contacts. According to this figure, material A is fixed and θ angle is increased to determine the friction coefficient between faces of materials A and B . Once the B matter moves with constant speed at angle of θ_1 , the kinetic friction coefficient of faces of two materials is obtained by $\tan(\theta_1)$.

The thickness of interface element is 0.01 mm. Experimental fracture energy for 10 layers laminate listed in Table 1 is used for the input fracture toughness for cohesive formulation. The purpose of this study is simulation of ENF test for 16 layers and 22 layers laminates and estimation of

of initiation value of fracture energy by described method using experimentally determined fracture energy of 10 layer laminate.

According to ASTM D7905/D7905M-14 (2014), the initiation value of fracture energy is calculated at the time of maximum load in ENF test. At the maximum load, damage exists in a number of elements in front of initial crack. Thus the crack advance (δa) in Eq. (22) is calculated by sum of products of damage of elements and corresponding elements length at crack tip.

A mesh-refinement study has been performed for laminate with 22 layers by repeating the analysis for two different mesh sizes. The element-length/rollers-distance ratios (L_e/L_r) of 0.01 and 0.001 used are shown in Fig. 9. The coordinate system has also been shown in Fig. 9. All rollers are fixed for rotation. Supporting rollers are also fixed at x and y directions and displacement of -4 mm in y direction has been applied to the loading roller.

The load-displacement plots obtained from experimental result and the simulation of 22 layers ENF specimen with two different mesh sizes are shown in Fig. 10. The maximum load has been dropped by 5% by decreasing the ratio of L_e/L_r from 0.01 to 0.001. The obtained response for simulation with L_e/L_r of 0.01, is stiffer due to the rough estimation of deformations. The obtained results show reasonable agreement with experiment results for simulation with L_e/L_r of 0.001.

The ENF test has been also simulated for laminate with thickness of 16 layers by the L_e/L_r of 0.001 using the input fracture toughness of 10 layers laminate obtained from experiment. The load-displacement plots obtained from experimental result and the simulation of 16 layers ENF

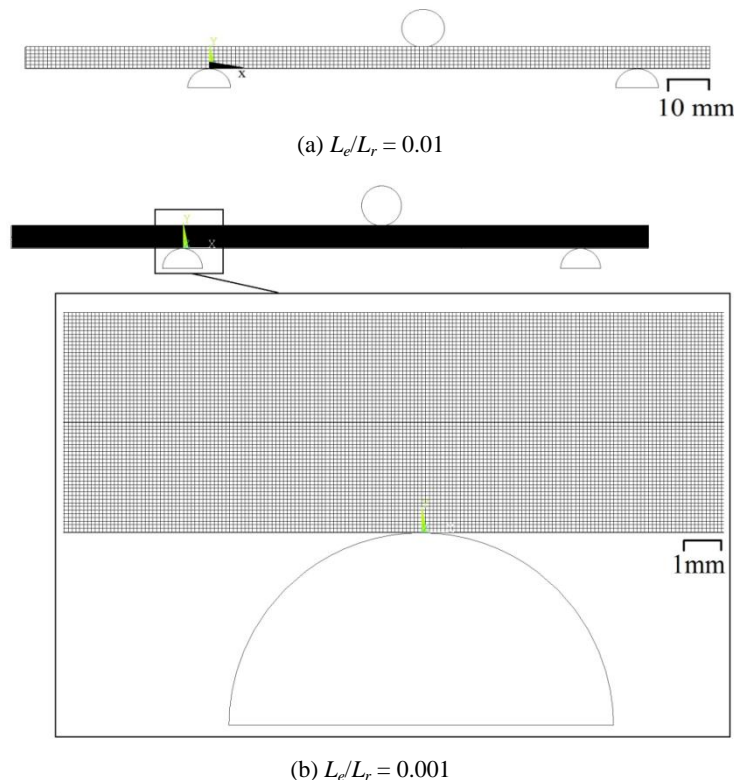


Fig. 9 The used two meshes in ENF specimens

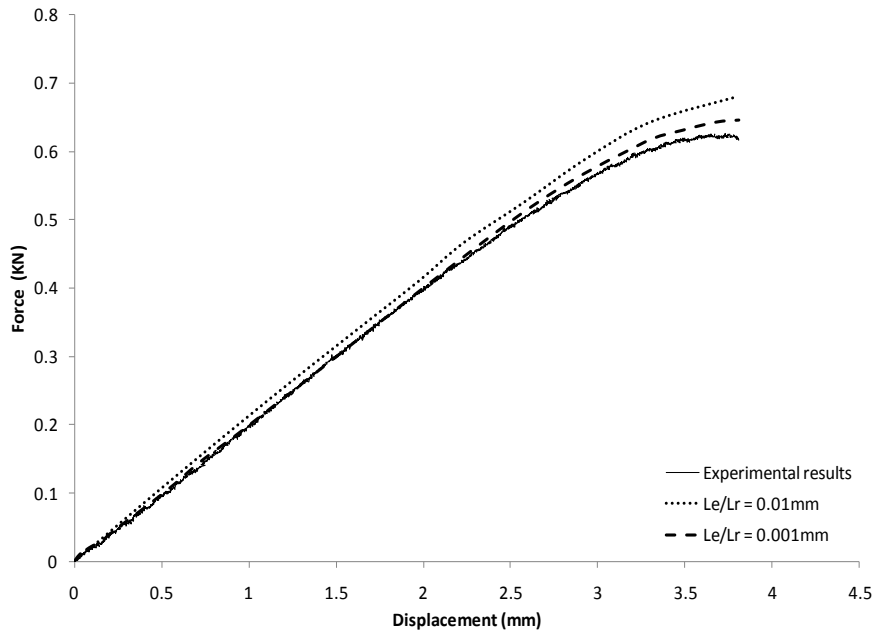


Fig. 10 Load displacement response of 22 layers ENF specimen using two different mesh sizes in comparison with experimental results

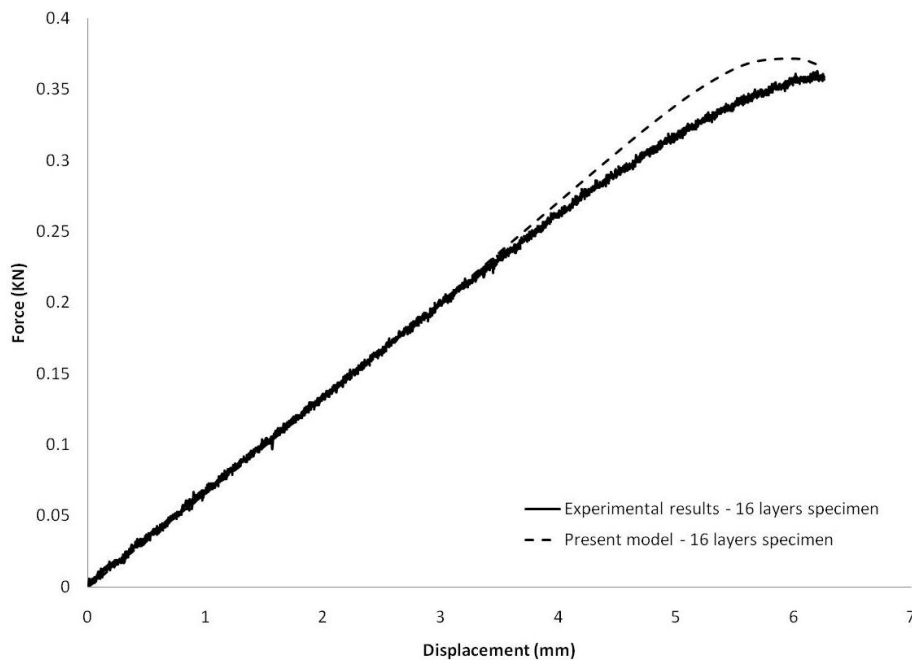


Fig. 11 Load displacement response of 16 layers ENF specimen in comparison with experimental results

specimen are shown in Fig. 11. One of the reasons for difference between the experiments and simulations could be measurement errors in experiments. Furthermore matrix cracking increases in the zone of loading and supporting rollers by increasing applied displacement. This leads to increase in the differences between the simulation and experimental curves. The determined fracture energies from simulations by described approach (modified DEBA) are compared with experiments in Fig. 12. It shows that the described approach is capable of estimating increase in fracture energy due to size effect. Increasing the thickness

from 16 to 22 layers led to 12% and 13% increase in obtained fracture energy in experiments and simulations respectively. The obtained initiation values of fracture energies by present method for laminates with 16 and 22 layers have 3.8% and 4.6% error in comparison with experiments. This shows reasonable agreement of the obtained results by the present method and the experiments. Including matrix cracking in the simulations as another mechanism of energy dissipation could increase the accuracy of the results.

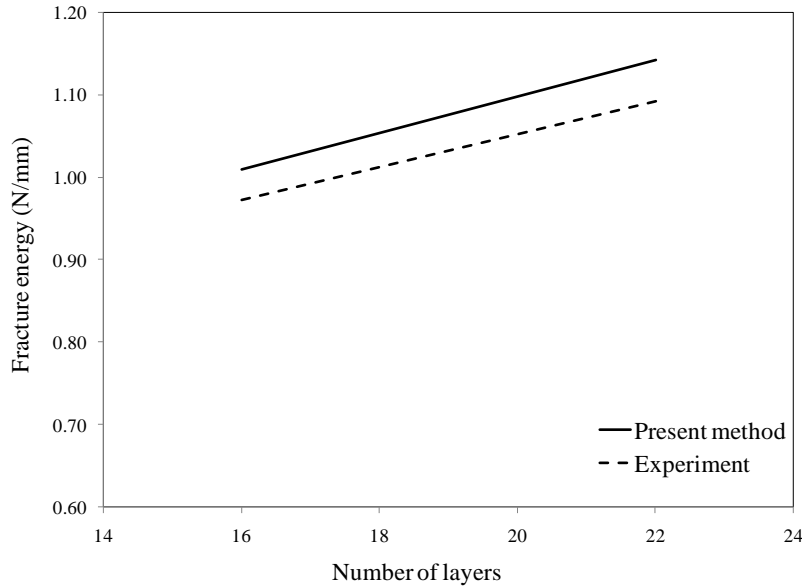


Fig. 12 Influence of thickness on obtained fracture energy of ENF specimen in comparison with experiments

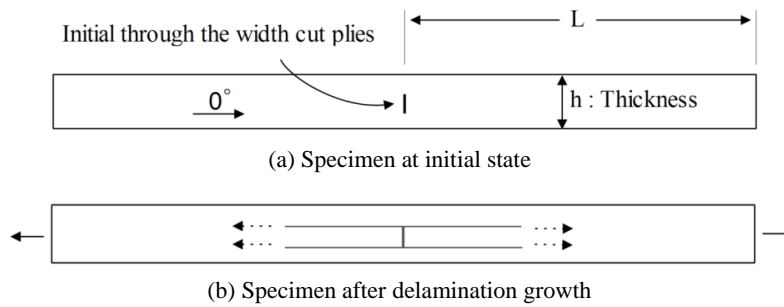


Fig. 13 The transverse crack tension (TCT) test specimen

4.3 Transverse crack tension simulation

In this section the measured shear fracture energy by TCT available experiments (Cui *et al.* 1994) have been compared with the results of analyses presented here. The TCT test consists of a unidirectional laminate with through the width cut plies under tension loading in fiber direction. Delamination propagates from the cut plies (Fig. 13) after a critical load. The load at the onset of delamination propagation is a measure for the initiation value of mode-II fracture energy. In this section, the measured fracture energy by the present approach has been compared with available experimental data (Cui *et al.* 1994) for different specimen's thicknesses.

The laminate is made of E-glass/913 epoxy. Material properties, friction coefficient and input parameters of E-glass/913 epoxy are listed in Table 3. These properties are taken from Cui *et al.* (1994) and Van der Meer and Sluys (2013) for the same material. The thickness of interface element is 0.01 mm.

Due to the existed symmetry conditions for the specimen, a quarter of that has been modeled. The length of the specimen ($2L$) in the experiments was 200 mm. The considered half length of the specimen (L) in the simulations is 12 mm. According to the previous results

(van der Meer and Sluys 2013), further increase of specimen length did not significantly influence the predicted delamination stress (stress at which initial delamination propagates). The width of the specimen is 10 mm. All specimens are unidirectional with 0° plies orientation with cut plies at the middle of the thickness and continuous plies above and below the cut plies. The material is E-glass epoxy with the material parameters presented in Table 3. Four types of laminates with different numbers of cut plies (n_{cut}) and continuous plies were considered in the modeling (1 cut /4 continuous, 2 cuts /8 continuous, 4 cuts /16 continuous, and 8 cuts /32 continuous). The ply thickness was equal to 0.127 mm. According to the previous mesh refinement and parametric study on TCT (van der Meer and Sluys 2013), the results with hardening modulus of 3 MPa for the this material and element length of 0.005 mm at crack tip best fits the experimental delamination stress. The mesh and coordinate system of the '2 cut /8 continuous' specimen is presented in Fig. 14. The boundary conditions according to the coordinate system shown in Fig. 14 are; at $x = 0$ for nodes at continuous plies, the degree of freedom has been constrained in x direction (plane of symmetry). At $y = 0$ the degree of freedom of all nodes has been constrained in y direction (plane of symmetry). Displacement of 2.4 mm has

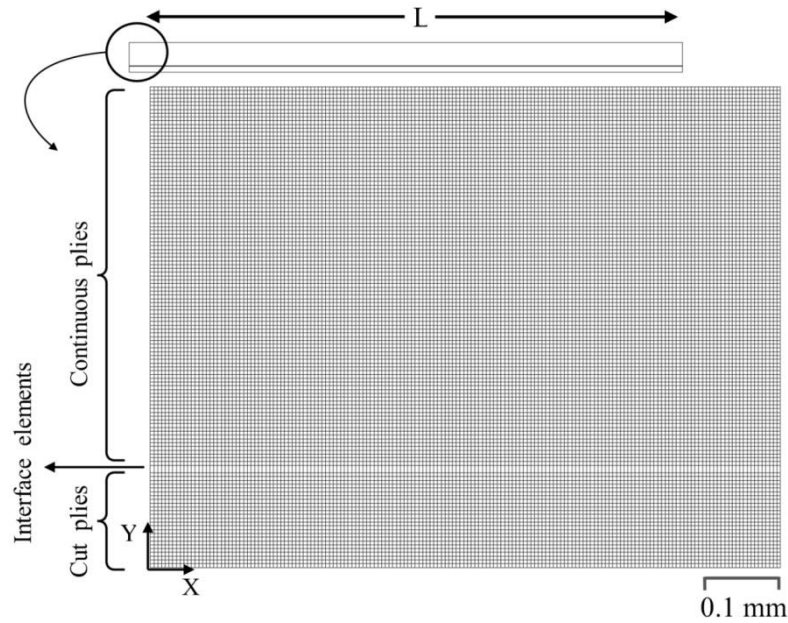


Fig. 14 Mesh of the '2 cut / 8 continuous' TCT specimen

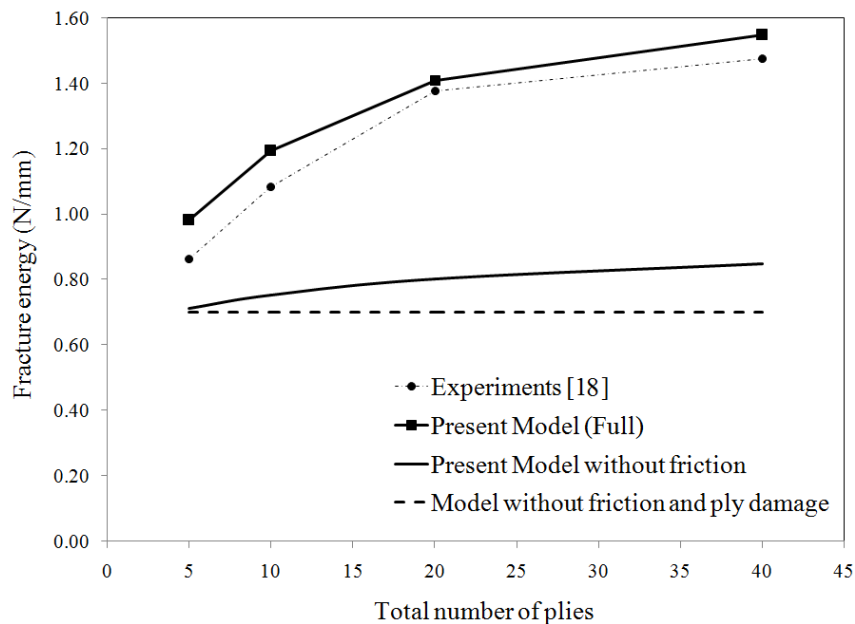


Fig. 15 Influence of thickness on measured fracture energy for TCT specimen

been applied for all nodes at $x = L$.

The influence of four different thicknesses on the initiation value of fracture energy has been examined (Fig. 15). Increasing the number of cut plies from $n_{\text{cut}} = 1$ (with total 5 plies) to $n_{\text{cut}} = 8$ (with total 40 plies) led to increase of fracture energy by 57.8%. The numerical results shown in Fig. 15 show the same range and order of the experimental measurements (provided in Cui *et al.* (1994)) verifying the formulations and modeling procedure. To study the effect of the cohesive friction in the formulation, the simulations were repeated once again with zero friction coefficient of cohesive zone and the results are depicted in

Fig. 15. The fracture energy has been increased by 19.2% from $n_{\text{cut}} = 1$ to $n_{\text{cut}} = 8$ for the model without friction. However existence of friction increases the effect of shear damage/plasticity model on the obtained results due to the increase in shear stress. Moreover the simulations have been repeated with zero friction coefficient in the interface and linear orthotropic material properties (without the ply damage/plasticity model) in the ply elements and the results are also depicted in Fig. 15. As it has been expected, the obtained fracture energies do not increase by increasing the thickness for the numerical simulations without friction and ply damage/plasticity model.

5. Conclusions

In this paper a modified direct energy balance approach developed to estimate the initiation fracture energy in composite laminates for different thickness using CZM and finite element modeling. Experimental results presented for characterization and ENF tests. The obtained results for ENF specimen showed that, by increasing the thickness from 16 plies to 22 layers, the fracture energy increased by 13%. It was shown that the described method is capable of estimating increase in fracture energy due to size effect. Reasonable agreement existed between obtained results for ENF specimens by experiments and simulation. It has been suggested that to increase the accuracy of the results, matrix cracking could be included in the simulation as another mechanism of energy dissipation. Numerical simulations of TCT specimens were also performed for four laminates thicknesses. Reasonable agreement was existed between the obtained results for TCT simulations by presented model and available experimental results in the literature. Therefore the presented formulations and developed procedure in this study can be used to estimate mode II shear fracture energy for different thickness from the available experiment that has already been done on a specific thickness.

References

- Achillopoulou, D.V., Kiziridou, A.N., Papachatzakis, G.A. and Karabinis, A.I. (2016), "Investigation of interface response of reinforced concrete columns retrofitted with composites", *Steel Compos. Struct., Int. J.*, **22**(6), 1337-1358.
- Alfano, G. and Sacco, E. (2006), "Combining interface damage and friction in a cohesive zone model", *Int. J. Numer. Methods Eng.*, **68**(5), 542-582.
- ASTM D7905/D7905M-14(2014), Standard Test Method for Determination of the Mode II Interlaminar Fracture Toughness of Unidirectional Fiber-Reinforced Polymer Matrix Composites; American Society for Testing and Materials International, West Conshohocken, PA, USA
- Barenblatt, G. (1959), "The formation of equilibrium cracks during brittle fracture. General ideas and hypotheses. Axially-symmetric cracks", *J. Appl. Math. Mech.*, **23**(3), 622-636.
- Barenblatt, G.I. (1962), "The mathematical theory of equilibrium cracks in brittle fracture", *Adv. Appl. Mech.*, **7**(1), 55-129.
- Bocciarelli, M., Colombi, P., Fava, G. and Sonzogni, L. (2016), "Energy-based analytical formulation for the prediction of end debonding in strengthened steel beams", *Compos. Struct.*, **153**, 212-221.
- Camanho, P.P., Davila, C.G. and De Moura, M.F. (2003), "Numerical simulation of mixed-mode progressive delamination in composite materials", *J. Compos. Mater.*, **37**(16), 1415-1438.
- Chaboche, J.L., Girard, R. and Schaff, A. (1997), "Numerical analysis of composite systems by using interphase/interface models", *Comput. Mech.*, **20**(1), 3-11.
- Cui, W., Wisnom, M.R. and Jones, M. (1994), "An experimental and analytical study of delamination of unidirectional specimens with cut central plies", *J. Reinf. Plast. Compos.*, **13**(8), 722-739.
- Davidson, B.D., Sun, X. and Vinciguerra, A.J. (2007), "Influences of friction, geometric nonlinearities, and fixture compliance on experimentally observed toughnesses from three and four-point bend end-notched flexure tests", *J. Compos. Mater.*, **41**(10), 1177-1196.
- Giroto, F., Dau, F. and Gutiérrez-Orrantia, M.E. (2017), "New analytical model for delamination of CFRP during drilling", *J. Mater. Process. Technol.*, **240**, 332-343.
- Hosseini-Toudeshky, H., Goodarzi, M.S. and Mohammadi, B. (2013), "Prediction of through the width delamination growth in post-buckled laminates under fatigue loading using de-cohesive law", *Struct. Eng. Mech., Int. J.*, **48**(1), 41-56.
- Hosseini-Toudeshky, H., Jahanmardi, M. and Goodarzi, M.S. (2015), "Progressive debonding analysis of composite blade root joint of wind turbines under fatigue loading", *Compos. Struct.*, **120**, 417-427.
- Kharazan, M., Sadr, M.H. and Kiani, M. (2014), "Delamination growth analysis in composite laminates subjected to low velocity impact", *Steel Compos. Struct., Int. J.*, **17**(4), 387-403.
- Kim, N., Kim, Y.H. and Kim, H.S. (2015), "Experimental and analytical investigations for behaviors of RC beams strengthened with tapered CFRPs", *Struct. Eng. Mech., Int. J.*, **53**(6), 1067-1081.
- Krueger, R. (2004), "Virtual crack closure technique: history, approach, and applications", *Appl. Mech. Rev.*, **57**(2), 109-143.
- Lin, G., Geubelle, P.H. and Sottos, N.R. (2001), "Simulation of fiber debonding with friction in a model composite pushout test", *Int. J. Solids Struct.*, **38**(46), 8547-8562.
- van der Meer, F.P.P. and Sluys, L.J.J. (2013), "A numerical investigation into the size effect in the transverse crack tension test for mode II delamination", *Compos. Part A Appl. Sci. Manuf.*, **54**, 145-152.
- Van Paepegem, W., De Baere, I. and Degrieck, J. (2006), "Modelling the nonlinear shear stress-strain response of glass fibre-reinforced composites. Part I: Experimental results", *Compos. Sci. Technol.*, **66**(10), 1455-1464.
- Rybicki, E.F. and Kanninen, M.F. (1977), "A finite element calculation of stress intensity factors by a modified crack closure integral", *Eng. Fract. Mech.*, **9**(4), 931-938.
- Shi, Y. and Soutis, C. (2016), "Modelling transverse matrix cracking and splitting of cross-ply composite laminates under four point bending", *Theor. Appl. Fract. Mech.*, **83**, 73-81.
- Shiming, C. and Huifen, Z. (2012), "Numerical analysis of the axially loaded concrete filled steel tube columns with debonding separation at the steel-concrete interface", *Steel Compos. Struct., Int. J.*, **13**(3), 277-293.
- Sun, X. and Davidson, B.D. (2005), "A direct energy balance approach for determining energy release rates in three and four point bend end notched flexure tests", *Int. J. Fract.*, **135**(1), 51-72.
- Sun, X. and Davidson, B.D. (2006), "Numerical evaluation of the effects of friction and geometric nonlinearities on the energy release rate in three-and four-point bend end-notched flexure tests", *Eng. Fract. Mech.*, **73**(10), 1343-1361.
- Turon, A., Costa, J., Camanho, P.P. and Dávila, C.G. (2007), "Simulation of delamination in composites under high-cycle fatigue", *Compos. Part A Appl. Sci. Manuf.*, **38**(11), 2270-2282.
- Tvergaard, V. (1990), "Effect of fibre debonding in a whisker-reinforced metal", *Mater. Sci. Eng. A.*, **125**(2), 203-213.
- Wisnom, M.R. (1992), "On the increase in fracture energy with thickness in delamination of unidirectional glass fibre-epoxy with cut central plies", *J. Reinf. Plast. Compos.*, **11**(8), 897-909.